Humanized mice with ectopic artificial liver tissues

Alice A. Chen[a,b,c], David K. Thomas[d,e], Luvena L. Ong[a], Robert E. Schwartz[c,f], Todd R. Golub[d,g,h], and Sangeeta N. Bhatia[a,c,f,h,i,1]

[a]Harvard-Massachusetts Institute of Technology Division of Health Sciences and Technology, Massachusetts Institute of Technology, 77 Massachusetts Avenue, Cambridge, MA 02139; [b]School of Engineering and Applied Sciences, Harvard University, 29 Oxford Street, Cambridge, MA 02138; [c]David H. Koch Institute for Integrative Cancer Research, Massachusetts Institute of Technology, 77 Massachusetts Avenue, Cambridge, MA 02139; [d]Broad Institute of Massachusetts Institute of Technology and Harvard, 7 Cambridge Center, Cambridge, MA 02142; [e]Division of Adult Palliative Care, Dana-Farber Cancer Institute and Harvard Medical School, 44 Binney Street, Boston, MA 02115; [f]Division of Medicine, Brigham and Women's Hospital, 75 Francis Street, Boston, MA 02115; [g]Department of Pediatric Oncology, Dana-Farber Cancer Institute and Harvard Medical School, 44 Binney Street, Boston, MA 02115; [h]The Howard Hughes Medical Institute, Massachusetts Institute of Technology, 77 Massachusetts Avenue, Cambridge, MA 02139; and [i]Department of Electrical Engineering and Computer Science, Massachusetts Institute of Technology, 77 Massachusetts Avenue, Cambridge, MA 02139

Edited by Mark A. Kay, Stanford University, Stanford, CA, and accepted by the Editorial Board June 2, 2011 (received for review February 2, 2011)

"Humanized" mice offer a window into aspects of human physiology that are otherwise inaccessible. The best available methods for liver humanization rely on cell transplantation into immunodeficient mice with liver injury but these methods have not gained widespread use due to the duration and variability of hepatocyte repopulation. In light of the significant progress that has been achieved in clinical cell transplantation through tissue engineering, we sought to develop a humanized mouse model based on the facile and ectopic implantation of a tissue-engineered human liver. These human ectopic artificial livers (HEALs) stabilize the function of cryopreserved primary human hepatocytes through juxtacrine and paracrine signals in polymeric scaffolds. In contrast to current methods, HEALs can be efficiently established in immunocompetent mice with normal liver function. Mice transplanted with HEALs exhibit humanized liver functions persistent for weeks, including synthesis of human proteins, human drug metabolism, drug–drug interaction, and drug-induced liver injury. Here, mice with HEALs are used to predict the disproportionate metabolism and toxicity of "major" human metabolites using multiple routes of administration and monitoring. These advances may enable manufacturing of reproducible in vivo models for diverse drug development and research applications.

Preclinical models provide a critical window into human physiology and are important for determining drug safety and efficacy. Bioengineering advances have produced in vivo platforms with improved disease modeling (1, 2), absorption, distribution, metabolism, excretion, and toxicity (ADME/Tox) (3, 4), and circulation-mimicking capabilities (4). "Human-on-a-chip" systems, however, show limited recapitulation of pharmacokinetics and cannot support clinically relevant administration routes. Elsewhere, humanized mice, based on genetic manipulation or transplantation of human cells, have also been highly enabling (5). Mice with chimeric livers show encouraging drug responsiveness (6, 7) and pathogen susceptibility (8–12). However, these models are confined to liver-injury, immunodeficient recipients and depend on the coordinated injection of high-quality human hepatocytes, which must home to the liver from the injection site, engraft, and expand over weeks to months within the injured host (13, 14). Given the limitations of current preclinical models, human metabolites and their downstream effects often go undetected until clinical trials, the most costly and dangerous phase of drug development (15).

Here we develop an improved humanized mouse model by implantation of tissue-engineered human ectopic artificial livers (HEALs). In the field of tissue engineering, polymeric scaffolds are widely used for cell and drug delivery in vivo (16, 17). Primary hepatocytes, however, are challenging to maintain and implant via biomaterials due to their unstable phenotype, variable engraftment efficiencies, and high metabolic needs (18). Use of partial hepatectomy with portal-caval shunt has been shown to improve hepatocyte engraftment and function in allogenic rat models (19, 20), suggesting that transplanted hepatocytes depend on signals (hepatotrophic factors) circulating from the portal vein. Despite these findings, support of implanted hepatocytes by sequential delivery of seeded cells, growth factors, hormones, and/or proangiogenic molecules has had limited success (21–24), and recent evidence showing promise for the survival of hepatocytes transplanted in the ectopic lymph node remains dependent on mouse liver injury (25). We hypothesized that an integrated system, based on hepatocyte encapsulation and the incorporation of juxtacrine and paracrine signals to stabilize the cell phenotype before, rather than during/after transplantation, could mitigate the requirement for portal venous flow or liver injury in vivo. To pursue our hypothesis, we engineered HEALs, functionalized polymer scaffolds that encapsulate primary human hepatocytes within a supportive microenvironment, and tested their ability to become integrated with recipient mouse circulation and perform human hepatic functions (Fig. S1).

Results and Discussion

Engineering HEALs. We previously reported that the viability and functions of primary rat hepatocytes are critically modulated by cell–cell interactions with nonparenchymal fibroblasts within 3D biomaterials (26). Therefore, to engineer HEALs, we sought to determine whether these findings could be extended to primary human hepatocyte encapsulation. Cocultivation of primary human hepatocytes with J2-3T3 mouse fibroblasts (HEP/FIB) for 1 wk, followed by encapsulation in PEG diacrylate (PEG-DA) polymer scaffolds ($\sim 0.5 \times 10^6$ total encapsulated hepatocytes), led to sustained albumin secretion and urea synthesis, whereas hepatocytes encapsulated alone declined over 2–4 d of culture (Fig. 1 *B* and *C*). Next, to study the impact of cell-matrix interactions on encapsulated primary human hepatocytes, we used the tunability of the PEG scaffold chemistry to incorporate the functional fibronectin-derived monomeric peptide sequence "RGDS" or negative control peptide "RGES" into the scaffold (Fig. 1*A*). The presence of RGDS improved the synthetic and secretory functions of the encapsulated HEP/FIB by two- to threefold, as compared to RGES controls (Fig. 1 *B* and *C*). These data, taken with studies from our group, which profiled the integrin expression of primary hepatocytes in vitro (27), suggest a dependence on juxtacrine cell interactions in 3D and responsiveness to the RGDS ligand via the hepatocyte cell surface integrin, $\alpha_5\beta_1$. Notably, in exploring alternative primary cell sources for HEAL fabrication, we compared fresh and cryopreserved hepatocyte HEP/FIB and found that they showed comparable levels of func-

Author contributions: A.A.C. and S.N.B. designed research; A.A.C., D.K.T., and L.L.O. performed research; D.K.T., R.E.S., and T.R.G. contributed new reagents/analytic tools; A.A.C., L.L.O., and S.N.B. analyzed data; and A.A.C., L.L.O., T.R.G., and S.N.B. wrote the paper.

The authors declare no conflict of interest.

This article is a PNAS Direct Submission. M.A.K. is a guest editor invited by the Editorial Board.

[1]To whom correspondence should be addressed. E-mail: sbhatia@mit.edu.

This article contains supporting information online at www.pnas.org/lookup/suppl/doi:10.1073/pnas.1101791108/-/DCSupplemental.

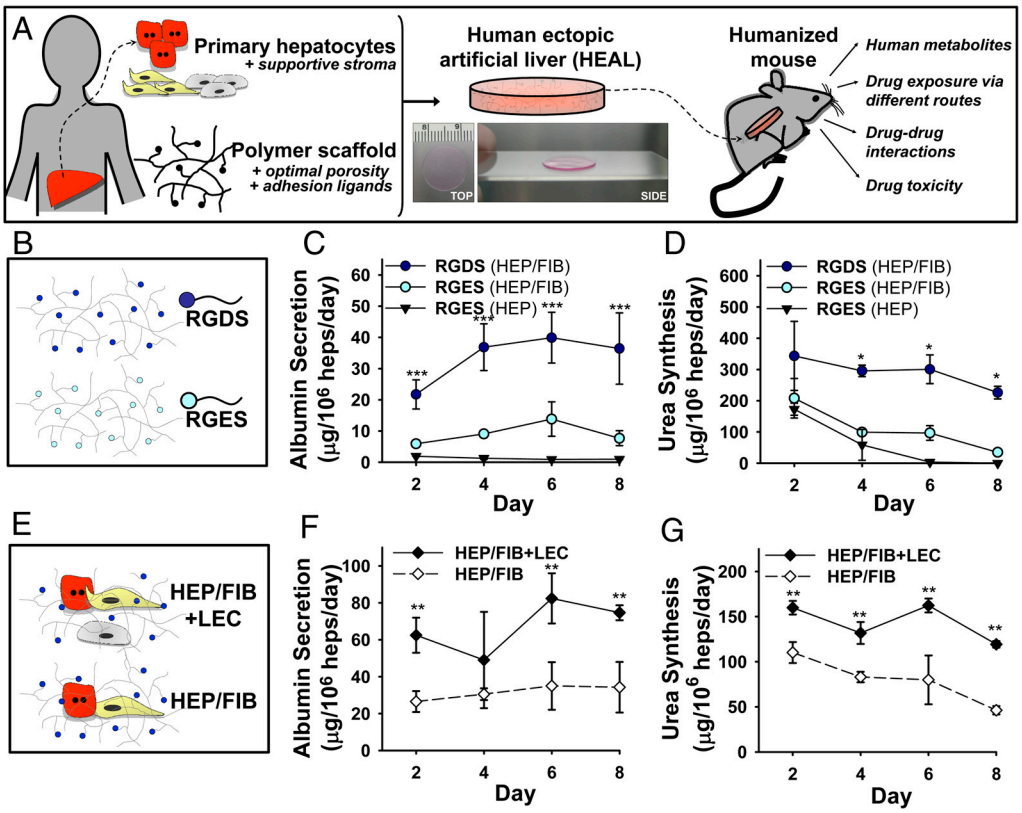

Fig. 1. Human ectopic artificial livers. (*A*) Schematic depicting the fabrication, implantation, and utility of HEALs for humanizing mice. Primary hepatocytes are cocultivated with stabilizing stromal fibroblasts on collagen-coated plates for 7–10 d, then encapsulated with liver endothelial cells in PEG-DA (20 kDa, 10% wt/vol) scaffolds derivatized with adhesion peptides. The resulting HEAL is approximately 20-mm diameter and 250-μm thick and comprises ~0.5×10^6 human hepatocytes (inset shows a 10-mm-diameter version from top and side views). After implantation into laboratory mice, engrafted and vascularized HEALs establish humanized models for drug development applications. (*B–D*) Covalent modification of PEG-DA hydrogels with peptide sequences RGDS (ligand) or RGES (negative control) (10 μmol/mL), and assessment of encapsulated primary HEP or HEP/FIB for albumin secretion (*C*) and urea synthesis (*D*) over time. (*E* and *F*) Coencapsulation of LEC with HEP/FIB cocultures in RGDS-derivatized PEG-DA hydrogels, and assessment of albumin secretion (*E*) and urea synthesis (*F*) over time. $*p < 0.01$, $**p < 0.05$, $***p < 0.001$ for $n = 6$ and SEM.

tional markers and viability staining after coculture and encapsulation (Fig. S2). Due to their availability and potential for improved reproducibility, subsequent HEALs were built from cryopreserved primary hepatocytes.

Human liver-derived nonparenchymal cells provide soluble signals important for hepatocyte development and maintenance (28). To investigate the effects of paracrine signaling on HEAL stability, we mixed human liver nonparenchymal cell lines with HEP/FIB clusters prior to encapsulation, entrapping HEP/FIB near, but not clustered with, the nonparenchymal cells (Fig. 1*D*). Coencapsulation of the human liver endothelial cell (LEC) line TMNK-1 (28, 29) was the most beneficial to rat hepatocellular function (Fig. 1 *E* and *F*), whereas additional mouse FIB were moderately and transiently supportive, and the human hepatic stellate cell (HSC) line TWNT-1 (30) had no effect (Fig. S3). The stabilizing influence of coembedded LECs was conserved between human and rat HEP/FIB cocultures, required initial cocultivation of HEP with FIB, and could not be reproduced with conditioned medium from cultured LECs (Fig. S4). Collectively, these data suggest that FIB provide critical spatiotemporal adhesive cues to help stabilize primary hepatocytes after isolation (31), whereas coembedded LEC may improve encapsulated cell function through secretion of short-range or rapidly turned over soluble factors. Ultimately, the optimization of cellular and chemical factors to provide juxtacrine and paracrine signaling within HEALs resulted in over 3 wk of human hepatic tissue function in vitro.

Characterization of HEALs for Drug Metabolism Gene Expression and Functions. In order to assess the utility of tissue-engineered hepatocyte cultures for drug metabolism studies, we characterized HEALs for the expression and function of human drug-metabolizing enzymes, comparing 3D-encapsulated HEP/FIB HEALs to same-donor 2D HEP/FIB cultures on day 10 of culture. The 2D condition acts as reference for a stable hepatocyte coculture model, previously shown to express a number of genes pertinent to ADME/Tox in vitro (32). However, to date, assessment of hepatocyte models has hinged on the measurement of only a small handful of drug-metabolizing enzymes. Noting that drug-metabolizing enzymes are regulated primarily at the level of transcription, we hypothesized that we could comprehensively assess drug-metabolizing enzyme expression levels in a low-cost, high-throughput assay based on the multiplexed ligation mediated amplification (LMA) of transcripts coupled to detection on Luminex beads (33). Accordingly, we designed probes for 83 human drug metabolism-encoding transcripts including phase I detoxification enzymes, phase II conjugating enzymes, phase III transporters, several key transcription factors, and albumin (Fig. 2*A* and Dataset S1). Comparing the relative gene expression between 2D and 3D cultures for two donors in independent experiments, we found that on average 7/7 nuclear receptors, 34/36 phase I [including cytochrome P450 superfamily enzymes (CYP450s)], 11/22 phase II, and 16/17 phase III genes showed similar or higher levels of expression in 3D HEP/FIB HEALs, compared to the 2D HEP/FIB control (Fig. 2*B*). Importantly, CYP3A4, 1A2, 2D6, 2E1, and the 2C isoforms, which collectively metabolize >90% clinical drugs, were expressed in HEALs established from both donors. These results indicate that relevant human enzymes are expressed in 2D and 3D hepatocyte cocultures and lay groundwork for future comprehensive and patient-specific profiling of drug-metabolizing enzyme expression and induction. To functionally validate the gene expression studies and to test the utility of HEALs for predicting clinical drug metabolism and interactions, we focused on one donor cell type and treated optimized (HEP/FIB + LEC) HEALs with omeprazole (OME) or rifampin (RIF), inducers of CYP1A2 and CYP3A4, respectively, and assessed CYP450 enzymatic activity upon exposure to known substrates (Fig. 2*C*). Compared to the vehicle control, OME induced CYP1A2-mediated metabolism of ethoxyresorufin (ER) by 11.5 ± 2.0-fold, but had only a minimal effect on the CYP3A4-mediated metabolism of testosterone (TEST). Conversely, RIF induced the metabolism of TEST by 13.7 ± 2.9-fold, but had no effect on the metabolism of ER. HEALs also recapitulated

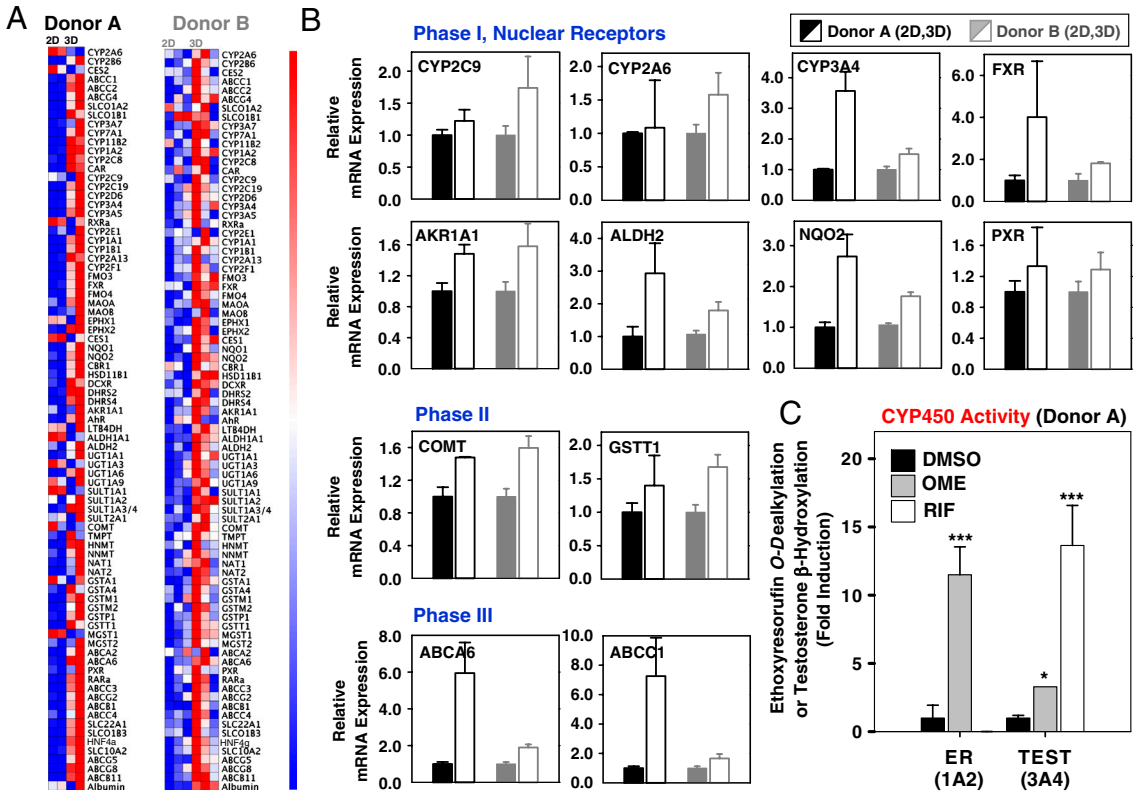

Fig. 2. Characterization of HEALs for drug metabolism gene expression and functions. (*A*) Heat map displays of LMA-Luminex analysis for 83 human-specific drug metabolism genes and transcription factors, shown separately for independent experiments analyzing different hepatocyte donors (donor A or B). Columns represent replicate loadings of RNA extracted from 2D HEP/FIB cultures ("2D") or 3D HEP/FIB HEALs ("3D") on day 10 postencapsulation. mRNA expression is determined relative to average of control gene transferrin, and heat maps are row-normalized to distinguish relative 2D to 3D differences. (*B*) Select gene sets comparing the relative mRNA expression of 3D HEP/FIB HEALs (open bars), normalized to 2D HEP/FIB cultures (filled bars) for phase I, nuclear receptors, phase II, and phase III drug metabolism genes after DMSO exposure. Data represent the mean and SEM of Luminex-loaded replicates for donor A (black) and donor B (gray). (*C*) CYP450 activity, induction, and drug interactions in day 6 3D HEP/FIB+LEC HEALs from donor A, treated with clinical inducers OME (40 μM) or RIF (25 μM) in vitro. Cultures were treated daily with inducers for 3 d before incubation with ER or TEST, conventional substrates for CYP1A2 and 3A4, respectively. Fold-induction of CYP450 activity was determined by normalization to DMSO control. By Student's *t* test, $*p < 0.01$, $***p < 0.001$ for $n = 4$ and SD.

clinically relevant drug–drug interactions involving CYP2A6- and CYP2D6-inhibiting compounds (Fig. S5). Thus, HEALs express functional human drug-metabolizing enzymes and show potential for screening compounds for CYP450 inducer, inhibitor, or effector responses.

Humanized Mice via Implantation of HEALs. We next sought to test whether stabilized HEALs could be implanted and functionally maintained in mice. We encapsulated HEP/FIB + LEC expressing luciferase under the human albumin promoter (Fig. S6) and transplanted the resulting reporter HEALs in the subcutaneous or intraperitoneal site of athymic nude mice (Fig. 3*A*). Whole-animal bioluminescence imaging and quantification of luciferase production indicated that the intraperitoneal site could support hepatic survival and albumin promoter activity for several weeks (Fig. 3 *A* and *B*), and up to 3 mo in one cohort of five mice (Fig. 3*A*). Serum analysis from HEAL-humanized mice confirmed the production and secretion of human proteins, albumin, and alpha-1-antitrypsin (Fig. 3*C* and Fig. S7). Based on qualitative inspection of vessels supplying the implants at day 6 or greater, engraftment of HEALs in vivo was highly efficient (91.6% of $n = 131$ mice transplanted). Vascular casting at day 35, followed by microcomputed tomography (micro-CT) angiography of extracted HEALs, confirmed host vessel recruitment to, around, and penetrating the implant (Fig. 3*D*–*F* and Movie S1). Together, these results demonstrate that stabilizing hepatocytes prior to implantation protects cells from death due to anoikis, loss of cellular signaling, and/or compromised oxygen transport during engraftment, and also decreases dependence on hepatotrophic factors from the portal vein. These advances enable rapid (<1 wk) and reproducible generation of HEAL-humanized mice using cryopreserved hepatocytes from different primary donors (Fig. 4 *A* and *B* and Fig. S8). In contrast, humanizing mice by current cell transplantation methods requires 2–6 mo and results in unpredictable and highly variable repopulation yields (ranging from single-digit to nearly complete percent humanization). Furthermore, current humanized mice are limited to liver-injury strains, whereas humanization with HEALs could be achieved in multiple strains (Swiss–Webster, C57/BL6) of immunocompetent, non-liver-injury mice for up to 8 d (Fig. 4*C*).

Prediction of Human Metabolites. The drug-metabolism profile of HEALs and the relatively facile generation of humanized mice through their implantation suggested the potential for in vivo preclinical studies. Major metabolites can pass undetected in standard animal models due to differences in drug metabolism pathways among species. Upon discovery in man, major metabolites require new preclinical phase evaluation and contribute to an alarming rate of prelaunch failures (15). To assess whether mice with HEALS could be used for early identification of major metabolites, we challenged wild-type and humanized athymic nude or immunocompetent C57/BL6 mice with drugs known to be metabolized differently by mice and humans. Coumarin, a CYP2A6 substrate, is primarily metabolized by humans to 7-hydroxycoumarin (7-HC), but preferentially metabolized in mice to coumarin-3,4-expoxide by cyp1a1/2 and 2e1 isoforms (34). Deb-

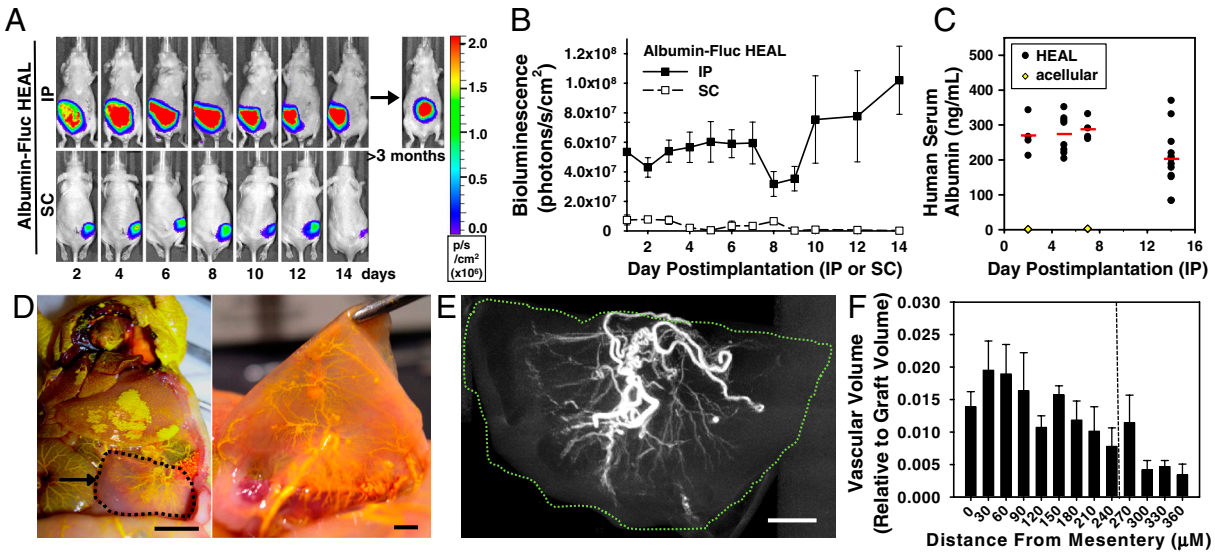

Fig. 3. Humanized mice via ectopic implantation of HEALs and functional assessment in vivo. (*A*) In vivo bioluminescence imaging and (*B*) quantification of reporter albumin-firefly luciferase (Fluc) HEALs implanted in the intraperitoneal cavity (IP) or subcutaneous space (SC) of athymic nude mice ($n = 8$ for IP, $n = 3$ for SC implants). Reporter albumin-Fluc HEALs were fabricated using HEP/FIB cocultures transduced by lentivirus to express luciferase under the human albumin promoter, prior to encapsulation with LEC (HEP/FIB + LEC). (*C*) Human serum albumin detected in mice humanized with intraperitoneal HEALs. Red bars mark average human serum albumin levels at each timepoint for $n = 6$ to 8 mice. (*D*) Representative photographs of mice with HEAL, perfused with yellow Microfil silicone rubber on day 35 after implantation. HEAL is shown pseudooutlined and exposed within peritoneal cavity (arrow; *Left*), and partially dissected (*Right*). (*E*) Micro-CT angiography scan and maximum intensity projection of representative extracted HEAL. (*F*) Quantification of vascular volume in extracted HEAL, based on 30-μm micro-CT slices from surface interfacing with host mesentery. The dashed line marks the expected opposite boundary surface of the HEAL based on its fabricated thickness of approximately 250 μm. (Scale bars: 5, 2, 5 mm.)

risoquine, a CYP2D6 probe, is metabolized to 4-hydroxydebrisoquine (4-OHDB) in humans and is not metabolized in mice (35). Importantly, human CYP2D6 is responsible for metabolism of 25% of known drugs and, due to its high number of polymorphisms, contributes to pronounced interindividual variability (up to 30–40-fold metabolic differences) (36). Indeed, debrisoquine hydroxylation genotyping and phenotyping can be used to classify patients as poor, intermediate, extensive, or ultrarapid metabolizers (36). We assessed CYP2D6 mRNA expression levels and debrisoquine hydroxylation activity of two human hepatocyte donors in vitro (Figs. 2*A* and 4*B*) and implanted HEALs derived from the poorer metabolizer into C57/BL6 mice. Following coumarin or debrisoquine exposure, serum and urine were analyzed by liquid chromatography (LC)/MS/MS to quantify parent drug and metabolite concentrations over time. Based on pharmacokinetic profiles, HEAL-humanized mice metabolized the parent compounds more efficiently than wild-type mice, as shown by higher metabolite C_{max} and area under the curve (AUC) values (Fig. 4 *D* and *E* and Fig. S9). For debrisoquine, the average humanized mouse metabolic ratio (metabolite AUC over parent AUC) fell within the range of debrisoquine hydroxylation in humans. For coumarin, humanized mice underpredicted clinical hydroxylation pharmacokinetics by approximately twofold (37) (Fig. 4*F*), possibly due to the contribution of murine CYP2A6 expressed in nonhepatic tissues (38). Nonetheless, HEAL-humanized mice correctly revealed both 7-HC and 4-OHDB as major human metabolites (metabolic ratio of >0.1) (15) (Fig. 4*F*). Thus, whereas standard mouse toxicology models would miss these breakdown products, HEAL-humanized mice could prevent the premature advancement and ultimate failure of such potentially problematic drugs in clinical trials.

Prediction of Drug–drug Interactions. We next characterized the ability of HEAL-humanized mice to probe clinical drug–drug interactions. Drug–drug interactions are critical determinants of drug efficacy and safety due to the potential for CYP450-inducing or CYP450-inhibiting drugs to alter the therapeutic or toxic effect of concomitantly administered compounds. We systemically exposed HEAL-implanted animals to the CYP3A4 inducer, RIF, and assessed the downstream effects by analyzing explanted HEALs. In response to intraperitoneal RIF, the enzymatic activity associated with explanted HEALs exposed to a second drug—CYP3A4 substrates 7-benzyloxy-4-trifluoromethylcoumarin (BFC) or TEST—was greater than fivefold induced as compared to DMSO-treated HEALs (Fig. 4*H* and Fig. S10). CYP1A2 activity, as probed by metabolism of the drug ER, was not altered by RIF, confirming the specificity of the inducer (Fig. 4*H*). These results indicate that HEALs can recapitulate the interaction of drug pairs and highlight the utility of HEAL explant following mouse exposure as a facile assay for drug–drug interactions.

To explore the utility of humanized mice for modeling toxic drug–drug interactions in vivo, we dosed RIF-induced or noninduced (DMSO-treated) animals with therapeutic levels of acetaminophen (APAP) and monitored human hepatotoxicity by assay of the mouse serum. APAP is a common analgesic that is severely hepatotoxic at high doses due to the CYP450-mediated formation of the reactive metabolite *N*-acetyl-p-benzoquinone (NAPQI); it is innocuous at therapeutic doses due to detoxification of NAPQI by cellular glutathione (39). Four hours after oral administration of APAP, mice that had been preinduced with RIF showed evidence of human hepatocellular injury, whereas mice exposed to APAP or RIF alone exhibited human serum albumin levels similar to untreated controls (Fig. 4*I* and Fig. S11). Mouse livers exposed to RIF, APAP, or RIF + APAP appeared uninjured based on serum liver enzyme tests and histopathological analysis (Fig. S12), consistent with recent findings on the species specificity of this drug interaction (40). These results indicate that HEAL-humanized mice can be useful for screening hepatotoxic drug–drug combinations and doses by multiple administration routes in vivo.

By leveraging tissue-engineering strategies to stabilize the functions of primary human hepatocytes within a biomaterial scaffold, we have established a unique humanized mouse model and demonstrated its utility for predicting human drug responses, pharmacokinetics upon multiple routes of administration, and metabolite formation in vivo. Unlike current transgenic and transplantation approaches, engineered HEAL-humanized mice

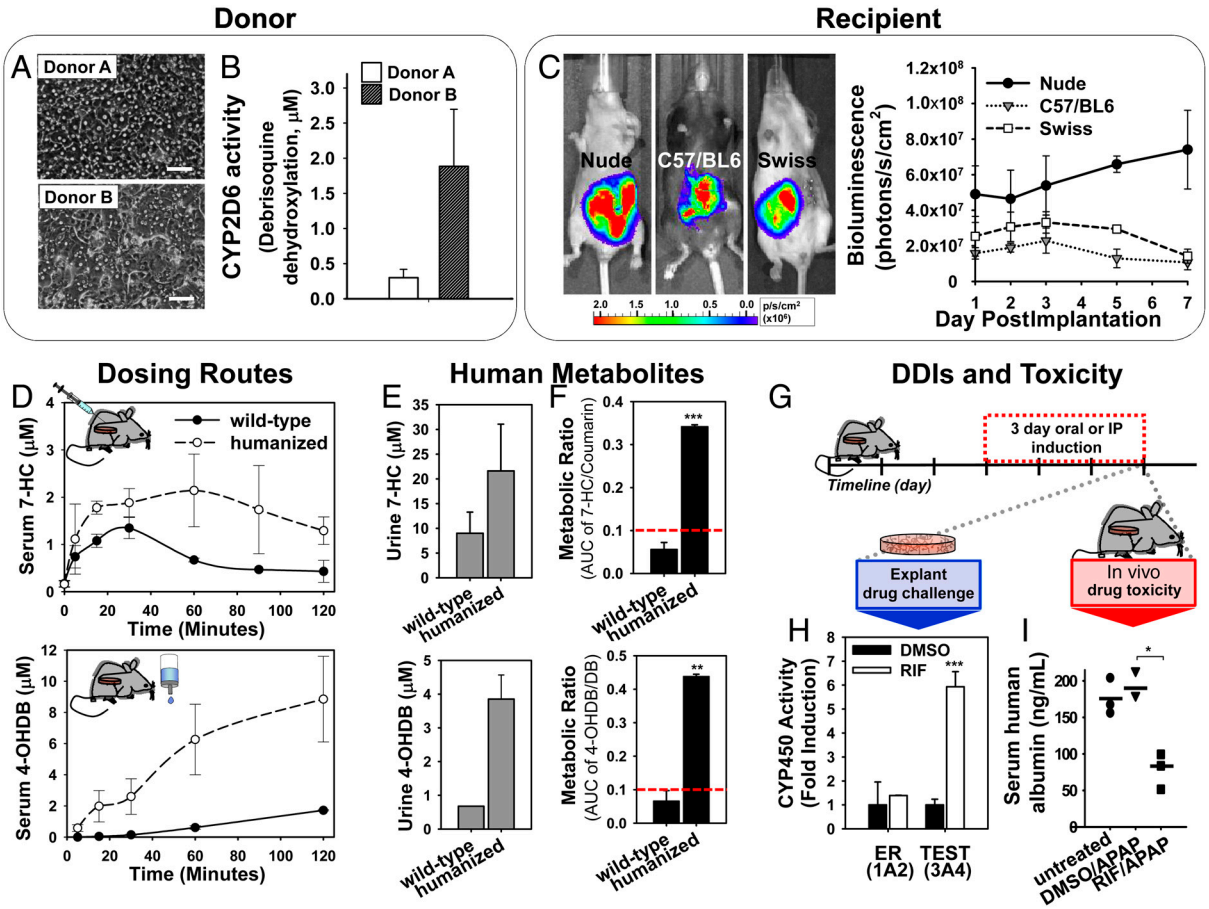

Fig. 4. Humanized mice using different donors or recipients. Drug dosing via multiple routes of administration and prediction of major human metabolites, drug–drug interactions, and toxicity. (*A*) Representative micrographs of cryopreserved primary hepatocytes from donors A and B, cocultivated with stromal fibroblasts for 7 d prior to 3D encapsulation. (Scale bar: 75 μm.) (*B*) Characterization of donors A- or B-derived HEALs for CYP2D6 activity by exposure to CYP2D6 substrate debrisoquine and quantification of debrisoquine hydroxylation. (*C*) In vivo bioluminescence imaging and quantification of reporter albumin-firefly luciferase HEALs from donor A, implanted in the intraperitoneal cavity of athymic nude, immunocompetent C57/BL6, or Swiss–Webster mice. Representative images 3 d after implantation are shown. (*D*) Pharmacokinetic analysis of serum metabolite 7-HC formation in humanized nude mice exposed to coumarin via i.p. injection (*Upper*), and serum metabolite 4-OHDB formation in humanized C57/Bl6 mice exposed to debrisoquine via oral gavage (*Lower*). (*E*) Detection of urinary 7-HC (*Upper*) or 4-OHDB (*Lower*) metabolite excretion over 4 h in vivo. (*F*) Identification of major human metabolites based on the metabolic ratio (MR; parent AUC over metabolite AUC). Red dashed line represents the lower threshold for classification as a major metabolite (0.1 MR). (*G*) Timeline of drug–drug interaction (DDI) study. Humanized mice ($n = 6$ per group) were administered RIF (25 mg/kg) daily for 3 d before (*H*) extraction of HEAL and incubation with CYP1A2 substrate ER or CYP3A4 substrate TEST ex vivo, or (*I*) in vivo oral exposure to APAP and serum assessment of human albumin production. Fold-induction of CYP450 activity was determined by normalization to DMSO. $^*p < 0.05$, $^{**}p < 0.01$, $^{***}p < 0.001$ for n as indicated and SEM. Error bars are SEM for $n = 3$ or greater.

can be generated rapidly (<2 wk), reproducibly, at high yields, and in the context of immunocompetent, non-liver-injury murine backgrounds. These advantages point to applications beyond drug safety, including investigations of human liver disease and hepatotropic infections, and potential integration with studies of normal mouse immunity or humanized immunity. We demonstrate the feasibility of implanting HEALs in immunocompetent mice for drug metabolism studies, and consider that the encapsulating polymer scaffold unique to this method of humanization may serve as not only a supportive microenvironment for hepatocytes but a delivery vehicle and potential rejection-delaying barrier (Fig. S13). HEAL-implanted mice may prove useful for the study of immune-mediated toxicity, idiosyncratic toxicity, and gut-liver interactions, and could include additional enabling features of tissue engineering such as multiplex donor screening (41). We envision that integration of this model into drug development pipelines has the potential to reduce clinical trial attrition rates and accelerate the process by which new therapeutics reach patients.

Materials and Methods

Fabrication and Culture of HEALs. HEALs were fabricated using a hydrogel polymerization apparatus (27). Briefly, prepolymer solution was loaded into a 20-mm diameter, 250-μm-thick silicone spacer and exposed to UV light from a spot curing system with collimating lens (320–390 nm, 10 mW/cm^2, 20–30 s; EXFO Lite). Prepolymer solution was composed of PEG-DA (20 kDa at 10% wt/vol; Laysan Bio), 0.1% wt/vol Irgacure 2959 photoinitiator (Ciba), and 10 μmol/mL acrylate-PEG-peptide monomers. Acrylate-PEG-peptide monomers were synthesized by conjugating RGDS or RGES (American Peptide) to acrylate-PEG-*N*-hydroxysuccinimide (3.4 kDa, JenKem) at a 1:1 molar ratio in 50 mM sodium bicarbonate buffer (pH 8.5). HEP/FIB cocultures were encapsulated at a final concentration of 8×10^6 hepatocytes per mL prepolymer, in the absence or presence of an additional 6×10^6 LEC/mL of prepolymer.

RNA Isolation and LMA-Luminex Analysis. Total RNA from three HEALs per donor was purified using Trizol (Invitrogen) and Mini-RNeasy kit (Qiagen) and pooled for analysis. LMA-Luminex procedures and probes are described in *SI Materials and Methods*. Data for replicate loadings, expressed in mean fluorescent intensity of at least 100 beads per sample, were scaled to the human transferrin gene and row-normalized for heat map representation using Gene Pattern open software (Broad Institute).

Implantation and Assessment of HEALs. HEALs were placed in the subcutaneous or peritoneal cavity of anesthetized NCr nude mice (Taconic) following a 1-cm incision. For noninvasive functional monitoring of transplanted HEALs, HEP/FIB cocultures were transduced with lentiviral pseudoparticles expressing firefly luciferase under the human albumin promoter (pTRIP.Alb.IVSb.IRES.tagRFP-DEST, 1:5 dilution; gift of John Schoggins and Charles Rice, The Rockefeller University, New York) prior to encapsulation.

Mice were administered 250 μL of 15 mg/mL D-Luciferin/PBS solution (Caliper Life Sciences) by intraperitoneal injection and imaged using the IVIS Spectrum (Xenogen) system and Living Image software (Caliper Life Sciences). The Committee for Animal Care in the Department of Comparative Medicine at Massachusetts Institute of Technology approved all animal procedures.

Vascular Perfusion and Micro-CT Imaging. Mice under isoflurane anesthesia were treated with intracardiac perfusions of 10 units/mL of heparin, 4 mg/L papaverin, and 1 g/L adenosine vasodilation agents, 2% (vol/vol) paraformaldehyde in PBS fixative, and Microfil silicon contrast reagent (yellow; FlowTech). Micro-CT scans were obtained using the explore Locus MicroCT platform (GE Healthcare; 0.021-mm voxel size, 400 views, 2,000-ms exposure, 80-kV photon energy, and 450-μA current) and analyzed using GE Microview and Osirix rending (Pixmeo Sarl) software.

Biochemical Assays. Human albumin or human alpha-1-antitrypsin was quantified by enzyme-linked immunosorbant assay using goat antihuman albumin or alpha-1-antitrypsin antibodies (Bethyl Labs). Urea was measured by acid- and heat-catalyzed detection of diacetylmonoxime conversion to a colorimetric product (StanBio Labs). Alanine aminotransferase and aspartate aminotransferase levels were detected with clinical kits (Teco Diagnostics).

Cytochrome-P450 Studies. All chemicals were purchased from Sigma. For induction studies, in vitro HEALs were treated daily for 3 d with CYP450 inducers 20 μM RIF or 50 μM OME in media (stocks <0.1% DMSO). Mice were injected intraperitoneally daily for 3 d with 25 mg/kg RIF/saline solution, or oral-gavaged daily for 3 d with 10 mg/kg OME/water solution. For inhibition studies, CYP450 inhibitors 8′methoxypsoralen (0–0.4 μM), or quinidine (0–1 μM) were incubated with HEALs in vitro at indicated concentrations for 1 h prior to addition of CYP450 substrates: BFC (50 μM), ER (5 μM) with 10 μM dicumarol, TEST (200 μM), coumarin (100 μM), or debrisoquine (DB, 100 μM), for 2 h at 37 °C with 5% CO_2. Glucuronidase/sulfatase-mediated phase II metabolites from coumarin or debrisoquine reactions were hydrolyzed by incubating with b-glucuronidase/arylsulfatase (Roche) for 2 h at 37 °C. The metabolites of BFC , ER, and coumarin were quantified at wavelengths 410/510, 530/590, 355/560 ex/emm, respectively. Substrates and metabolites of TEST, coumarin, and DB were quantified by LC/MS/MS (Apredica).

Pharmacokinetic Analysis. Mice administered 80 mg/kg of coumarin injected intraperitoneally or 2 mg/kg DB oral-gavaged were subjected to retroorbital draw at 5, 10, 15, 30, 60, 90, and 120 min and terminal urine collection at 4 h. Glucuronidase/sulfatase-mediated phase II metabolites were hydrolyzed with b-glucuronidase/arylsulfatase (Roche) for 2 h at 37 °C. Metabolites 7-HC and 4-OHDB were quantified using LC/MS/MS (Apredica). The area under the curve from time 0 until the last measurable plasma concentration ($AUC_{0\text{-}t}$) was calculated using the linear trapezoidal rule. Peak concentration (C_{max}) and time to reach maximum concentration (t_{max}) were obtained from the plasma concentration-time profile. Metabolic ratios were determined by dividing $AUC_{0\text{-}t}$ of metabolite by $AUC_{0\text{-}t}$ of the parent drug.

Statistical analysis. Experiments were independently repeated 2–3 times with replicate samples as indicated in figure captions. Statistical analysis was performed using one-way ANOVA and Tukey's post hoc test for group comparisons. Errors bars represent SEM.

ACKNOWLEDGMENTS. We gratefully acknowledge support from the National Institutes of Health (EB008396, DK56966), National Cancer Institute (RL1CA133834 to D.K.T.), Howard Hughes Medical Institute (S.N.B.), and National Defense Science and Engineering and National Science Foundation Graduate Research Programs (A.A.C.). We thank Steven Katz, Semmie Kim, and Sarah Han for technical assistance, Dr. Howard Green (Harvard University) for the 3T3-J2 line, Dr. Naoya Kobayashi (Okayama University) for the TMNK-1 (LEC) line, Dr. John Schoggins and Dr. Charles Rice (Rockefeller University) for the albumin-luciferase lentivirus construct, and Dr. Scott Malstrom (Massachusetts Institute of Technology) for animal imaging assistance. We also thank Dr. Salman Khetani (Hepregen), Dr. Robert Gould (Broad Institute), Dr. Thomas Baillie (University of Washington), Dr. Catherine Murray, Dr. Kelly Stevens, Dr. Sandra March, and Shengyong Ng for insightful discussions.

1. Huebsch N, Mooney DJ (2009) Inspiration and application in the evolution of biomaterials. *Nature* 462:426–432.
2. Ploss A, et al. (2010) Persistent hepatitis C virus infection in microscale primary human hepatocyte cultures. *Proc Natl Acad Sci USA* 107:3141–3145.
3. Khetani SR, Bhatia SN (2008) Microscale culture of human liver cells for drug development. *Nat Biotechnol* 26:120–126.
4. Sung JH, Kam C, Shuler ML (2010) A microfluidic device for a pharmacokinetic-pharmacodynamic (PK-PD) model on a chip. *Lab Chip* 10:446–455.
5. Shultz LD, Ishikawa F, Greiner DL (2007) Humanized mice in translational biomedical research. *Nat Rev Immunol* 7:118–130.
6. Tateno C, et al. (2004) Near completely humanized liver in mice shows human-type metabolic responses to drugs. *Am J Pathol* 165:901–912.
7. Katoh M, Yokoi T (2007) Application of chimeric mice with humanized liver for predictive ADME. *Drug Metab Rev* 39:145–157.
8. Brezillon N, Kremsdorf D, Weiss MC (2008) Cell therapy for the diseased liver: From stem cell biology to novel models for hepatotropic human pathogens. *Dis Model Mech* 1:113–130.
9. Morosan S, et al. (2006) Liver-stage development of Plasmodium falciparum, in a humanized mouse model. *J Infect Dis* 193:996–1004.
10. Ohashi K, et al. (2000) Sustained survival of human hepatocytes in mice: A model for in vivo infection with human hepatitis B and hepatitis delta viruses. *Nat Med* 6:327–331.
11. Mercer DF, et al. (2001) Hepatitis C virus replication in mice with chimeric human livers. *Nat Med* 7:927–933.
12. Bissig KD, et al. (2010) Human liver chimeric mice provide a model for hepatitis B and C virus infection and treatment. *J Clin Invest* 120:924–930.
13. de Jong YP, Rice CM, Ploss A (2010) New horizons for studying human hepatotropic infections. *J Clin Invest* 120:650–653.
14. Legrand N, et al. (2009) Humanized mice for modeling human infectious disease: Challenges, progress, and outlook. *Cell Host Microbe* 6:5–9.
15. Leclercq L, et al. (2009) Which human metabolites have we MIST? Retrospective analysis, practical aspects, and perspectives for metabolite identification and quantification in pharmaceutical development. *Chem Res Toxicol* 22:280–293.
16. Karp JM, Langer R (2007) Development and therapeutic applications of advanced biomaterials. *Curr Opin Biotechnol* 18:454–459.
17. Tibbitt MW, Anseth KS (2009) Hydrogels as extracellular matrix mimics for 3D cell culture. *Biotechnol Bioeng* 103:655–663.
18. Davis MW, Vacanti JP (1996) Toward development of an implantable tissue engineered liver. *Biomaterials* 17:365–372.
19. Mooney DJ, et al. (1997) Long-term engraftment of hepatocytes transplanted on biodegradable polymer sponges. *J Biomed Mater Res* 37:413–420.
20. Kneser U, et al. (1999) Long-term differentiated function of heterotopically transplanted hepatocytes on three-dimensional polymer matrices. *J Biomed Mater Res* 47:494–503.
21. Kaihara S, et al. (2000) Silicon micromachining to tissue engineer branched vascular channels for liver fabrication. *Tissue Eng* 6:105–117.
22. Ohashi K, et al. (2005) Liver tissue engineering at extrahepatic sites in mice as a potential new therapy for genetic liver diseases. *Hepatology* 41:132–140.
23. Smith MK, Riddle KW, Mooney DJ (2006) Delivery of hepatotrophic factors fails to enhance longer-term survival of subcutaneously transplanted hepatocytes. *Tissue Eng* 12:235–244.
24. Yokoyama T, et al. (2006) In vivo engineering of metabolically active hepatic tissues in a neovascularized subcutaneous cavity. *Am J Transplant* 6:50–59.
25. Hoppo T, Komori J, Manohar R, Stolz DB, Lagasse E (2011) Rescue of lethal hepatic failure by hepatized lymph nodes in mice. *Gastroenterology* 140:656–666 e652.
26. Underhill GH, Chen AA, Albrecht DR, Bhatia SN (2007) Assessment of hepatocellular function within PEG hydrogels. *Biomaterials* 28:256–270.
27. Liu Tsang V, et al. (2007) Fabrication of 3D hepatic tissues by additive photopatterning of cellular hydrogels. *FASEB J* 21:790–801.
28. Soto-Gutierrez A, et al. (2006) Reversal of mouse hepatic failure using an implanted liver-assist device containing ES cell-derived hepatocytes. *Nat Biotechnol* 24:1412–1419.
29. Matsumura T, et al. (2004) Establishment of an immortalized human-liver endothelial cell line with SV40T and hTERT. *Transplantation* 77:1357–1365.
30. Watanabe T, et al. (2003) Establishment of immortalized human hepatic stellate scavenger cells to develop bioartificial livers. *Transplantation* 75:1873–1880.
31. Hui EE, Bhatia SN (2007) Micromechanical control of cell–cell interactions. *Proc Natl Acad Sci USA* 104:5722–5726.
32. Lerche C, et al. (1997) Regulation of the major detoxication functions by phenobarbital and 3-methylcholanthrene in co-cultures of rat hepatocytes and liver epithelial cells. *Eur J Biochem* 244:98–106.
33. Peck D, et al. (2006) A method for high-throughput gene expression signature analysis. *Genome Biol* 7:R61.1–R61.6.
34. Uehara T, et al. (2008) Species-specific differences in coumarin-induced hepatotoxicity as an example toxicogenomics-based approach to assessing risk of toxicity to humans. *Hum Exp Toxicol* 27:23–35.
35. Yu AM, Idle JR, Gonzalez FJ (2004) Polymorphic cytochrome P450 2D6: Humanized mouse model and endogenous substrates. *Drug Metab Rev* 36:243–277.
36. Zhou SF (2009) Polymorphism of human cytochrome P450 2D6 and its clinical significance: Part I. *Clin Pharmacokinet* 48:689–723.
37. Rautio A, Kraul H, Kojo A, Salmela E, Pelkonen O (1992) Interindividual variability of coumarin 7-hydroxylation in healthy volunteers. *Pharmacogenetics* 2:227–233.
38. Ding X, Kaminsky LS (2003) Human extrahepatic cytochromes P450: Function in xenobiotic metabolism and tissue-selective chemical toxicity in the respiratory and gastrointestinal tracts. *Annu Rev Pharmacol Toxicol* 43:149–173.
39. James LP, Mayeux PR, Hinson JA (2003) Acetaminophen-induced hepatotoxicity. *Drug Metab Dispos* 31:1499–1506.
40. Cheng J, Ma X, Krausz KW, Idle JR, Gonzalez FJ (2009) Rifampicin-activated human pregnane X receptor and CYP3A4 induction enhance acetaminophen-induced toxicity. *Drug Metab Dispos* 37:1611–1621.
41. Chen AA, Underhill GH, Bhatia SN (2010) Multiplexed, high-throughput analysis of 3D microtissue suspensions. *Integr Biol (Camb)* 2:517–527.

Supporting Information

Chen et al. 10.1073/pnas.1101791108

SI Materials and Methods

Cell Culture. Cells were cultured in a 5% CO_2 humidified incubator at 37 °C both before and after encapsulation. Fresh primary human hepatocyte suspensions (CellzDirect) were obtained from a 48-yr-old, nonobese Caucasian male with no history of smoking, alcohol, or drug abuse. Cryopreserved primary human hepatocytes were obtained from CellzDirect (donor A: Lot Hu4151, 50-yr-old female) or Celsis technologies (donor B: Lot GHA, 1-yr-old female). Primary rat hepatocytes were harvested from 2–3-mo-old adult female Lew rats (Charles River), as previously described (S1). Human hepatocyte medium was high glucose DMEM with 10% (vol/vol) FBS, 1% (vol/vol) ITS Premix (insulin, human transferrin, and selenous acid; BD Biosciences), 0.49 pg/mL glucagon, 0.08 ng/mL dexamethasone, 0.018 M Hepes, and 1% (vol/vol) penicillin-streptomycin. Rat hepatocyte medium contained high glucose DMEM (Invitrogen), 10% FBS (Invitrogen), 0.5 units/mL insulin (Lilly), 7 ng/mL glucagons (Bedford Laboratories), 7.5 μg/mL hydrocortisone (Sigma), 10 units/mL penicillin (Invitrogen), and 10 mg/mL streptomycin (Invitrogen).

J2-3T3 fibroblasts (gift of Howard Green, Harvard Medical School) were cultured at <18 passages in DMEM with high glucose, 10% (vol/vol) bovine serum, and 1% (vol/vol) penicillin-streptomycin. To prepare hepatocyte/fibroblast cocultures, hepatocytes were seeded at a density of 1.0×10^6 cells/well in a six-well plate adsorbed with 0.14 mg/mL Collagen-1 extracted from rat-tail tendons. Fibroblasts were added at 0.4×10^6 cells/well 24 h after hepatocyte seeding. Culture medium was changed daily for 7–10 d prior to hydrogel encapsulation or in vivo injection.

The liver endothelial cells (LEC) and hepatic stellate cell line are TMNK-1 and TWNT-1, respectively, and were established by and gifted from Naoya Kobayashi (Okayama University). Both lines were cultured at <18 passages in DMEM with high glucose, 10% (vol/vol) FBS, and 1% (vol/vol) penicillin-streptomycin.

Conditioned Media Experiments. LEC encapsulated at a density of 6×10^6 cells/mL prepolymer solution or the same number of cells seeded into a 12-well plate were cultured in 0.5 mL rat hepatocyte medium. Conditioned media from 2D monolayer LEC or 3D encapsulated LEC were used to feed 3D rat hepatocyte/J2-3T3 mouse fibroblast cocultures in 12-well plates daily, starting 1 day after human ectopic artificial liver (HEAL) fabrication. Supernatants were collected every 48 h and stored at −20 °C for hepatocellular assays.

1. Seglen PO (1976) Preparation of isolated rat liver cells. *Methods Cell Biol* 13:29–83.

Ligation Mediated Amplification (LMA)-Luminex analysis. LMA-Luminex procedures and probes for profiling 83 human-specific drug metabolism enzymes and three control human genes (Actin B, Albumin, Transferrin) were designed, developed, and characterized by David Thomas of the Broad Institute (see Dataset S1).

For LMA-Luminex analysis, total RNA (250 ng) was diluted in turbo capture lysis buffer (20 μL total), immobilized on a Qiagen turbo capture 384-well plate, and reverse-transcribed using oligo-dT priming. A solution containing FlexMap tag upstream probe, phosphorylated downstream probe, and ligation buffer was added and reacted at 95 °C for 2 min denaturation, 50 °C for 60 min annealing, 4 °C for 1 min cooling. Taq ligase was added and incubated at 45 °C for 60 min ligation. Universal PCR was performed for 35 cycles using a biotinylated T7 forward primer and T3 reverse primer in buffer with dNTPs and Taq polymerase. FlexMap microsphere beads conjugated with antitag oligonucleotides were added and allowed to hybridize in buffer at 45 °C for 60 min after a 2 min 95 °C denaturation step. Streptavidin-phyoerythrin was reacted at 45 °C for 5 min to capture amplicons, and 100 events per bead were analyzed for internal bead color and phyoerythrin reporter fluorescence on a Luminex FlexMap 3D analyzer.

Drug–Drug Interaction and Toxicity Studies. Humanized mice at day 6 after HEAL implantation were induced for 3 d by daily intraperitoneal injection of rifampin (25 mg/kg) or DMSO vehicle control. At day 9 after HEAL implantation, mice were fed by oral gavage with 500 μL drinking water or 500 μL acetaminophen (APAP, 250 mg/kg) in water. Mice were fasted for 16 h prior to APAP administration. Following APAP exposure, blood was collected by retroorbital draw at 4 h and serum analyzed for enzymatic activity of alanine aminotransferase and aspartame aminotransferase, non-species-specific markers of liver damage (Teco Diagnostics). HEALs and mouse livers were extracted for biochemical and histological analysis. Mouse livers were paraffin-embedded, sectioned with 5-μm slices, deparaffinized, and stained for hematoxylin and eosin.

Microscopy. Fluorescent images were acquired using a Nikon Ellipse TE200 inverted fluorescence microscope and CoolSnap-HQ Digital CCD Camera, with MetaMorph Image Analysis software package for acquiring digital micrographs. Histology images were acquired using a Zeiss Axiophot II upright microscope with color camera and OpenLab/Volocity software.

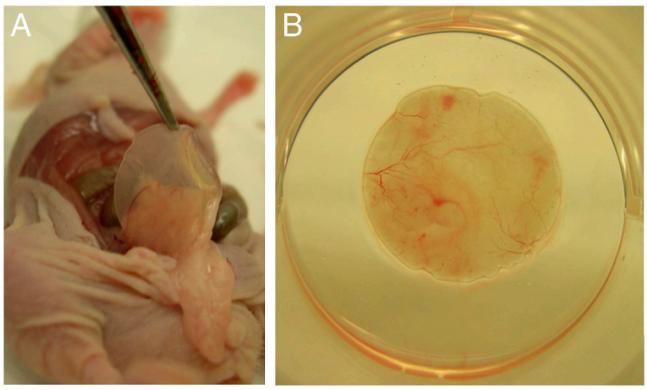

Fig. S1. Images of HEALs. (*A* and *B*) HEAL comprising human hepatocytes, fibroblasts, and liver endothelial cells encapsulated in PEG diacrylate + peptide sequence RGDS hydrogel (10-mm diameter, 250-μm thick), implanted in the intraperitoneal cavity of a nude mouse and extracted on day 7 of implantation. The HEAL is shown attached to the mouse mesentery tissue and partially extracted with forceps (*A*), or fully extracted into a 12-well tissue culture plate for macroscopic vessel visualization (*B*).

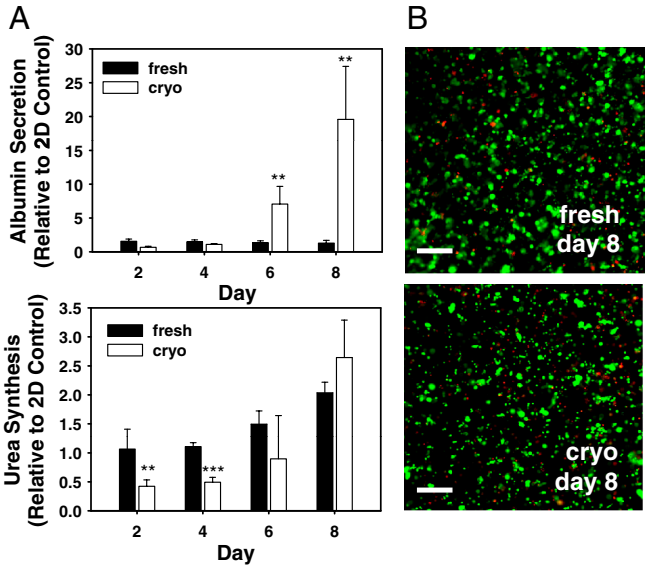

Fig. S2. Functional assessment and viability of HEALs fabricated from fresh versus cryopreserved primary human hepatocytes. (*A*) Fresh or cryopreserved primary human hepatocytes cocultivated with stromal fibroblasts on collagen plates for 7–10 d, then encapsulated in PEG diacrylate hydrogels (10% wt/vol, 20 kDa) derivatized with RGDS (10 μmol/mL). Albumin secretion and urea synthesis were measured over time in media from fresh (black bars) or cryopreserved (white bars) HEALs. Functions are reported relative to monolayer hepatocyte/fibroblast cocultures on collagen, to normalize donor- and isolation-specific variation among fresh, primary human hepatocyte sources. (*B*) Fluorescence micrographs of fresh (*Upper*) versus cryopreserved (*Lower*) HEALs treated with the green/red calcein acetoxymethyl ester/ethidium homodimer viability/death stain, 8 d after encapsulation. (Scale bar: 200 μm.) $^{**}p < 0.01$, $^{***}p < 0.001$ for $n = 6$ and SEM.

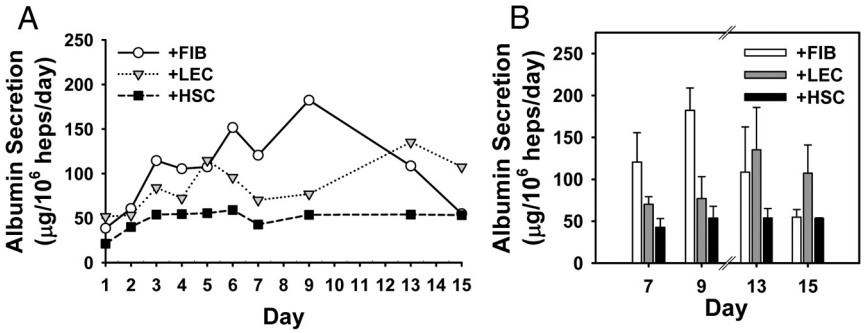

Fig. S3. Functional optimization of rat 3D HEP/FIB cultures by coencapsulation of additional fibroblasts (FIB), liver endothelial cell line (LEC), or hepatic stellate cell line (HSC) cells. (*A*) HEP/FIB cocultures (8×10^6 hep/mL) mixed with FIB, LEC, and HSC (6×10^6 cells/mL), encapsulated in PEG+RGDS hydrogels, and monitored for albumin secretion over 15 d. (*B*) Albumin secretion on days 7, 9, 13, and 15 after encapsulation; $n = 3$ per condition, with error bars representing SEM.

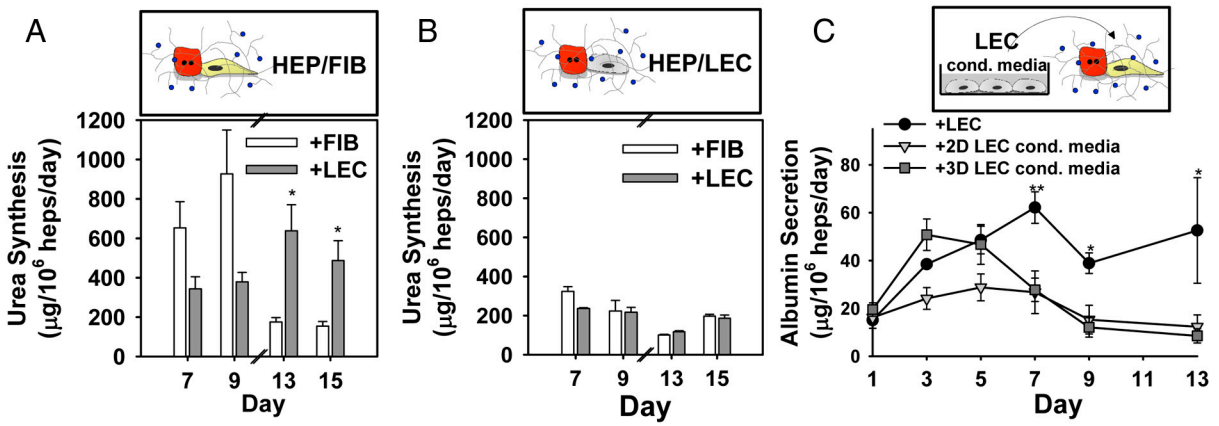

Fig. S4. Stabilizing effect of coencapsulated liver endothelial cells (LEC) is dependent on HEP/FIB contact and not reproduced by conditioned media. (*A*) Urea synthesis of HEALs made by coencapsulating primary rat HEP/FIB cocultures with additional liver endothelial cells (+LEC) or fibroblasts (+FIB). (*B*) Urea synthesis of HEALs made by coencapsulating primary rat HEP/LEC cocultures with additional +LEC or +FIB. (*C*) Albumin secretion of rat 3D HEP/FIB cultures fed daily with 2D or 3D LEC conditioned media. $*p < 0.05$, $**p < 0.01$, $***p < 0.001$ compared to control for $n = 4$ and SEM.

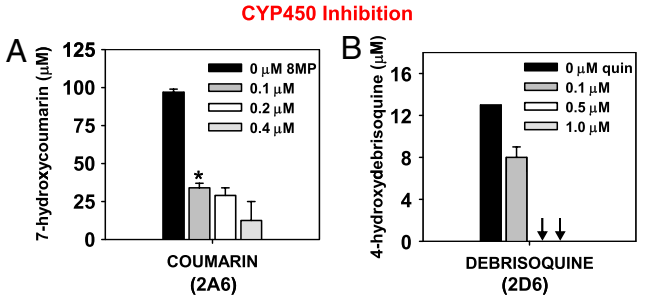

Fig. S5. Characterization of cytochrome P450 superfamily enzyme (CYP450) inhibition in HEALs. (*A*) HEALs treated with the clinical CYP2A6 inhibitor 8-methoxypsoralen (8MP) at 0, 0.1, 0.2, or 0.4 μM for 1 h before incubation with CYP2A6 substrate coumarin (100 μM for 2 h). Hydroxylation of coumarin to 7-hydroxycoumarin was measured by liquid chromatography (LC)/MS/MS against a standard curve. (*B*) HEALs treated with the clinical CYP2D6 inhibitor quinidine (quin) at 0, 0.1, 0.5, or 1.0 μM for 1 h before incubation with CYP2D6 substrate debrisoquine (100 μM for 2 h). Hydroxylation of debrisoquine to 4-hydroxydebrisoquine was measured by LC/MS/MS against a standard curve. Arrows represent values that were below the LC/MS/MS limit of detection. $*p < 0.05$ for $n = 2$ and SEM.

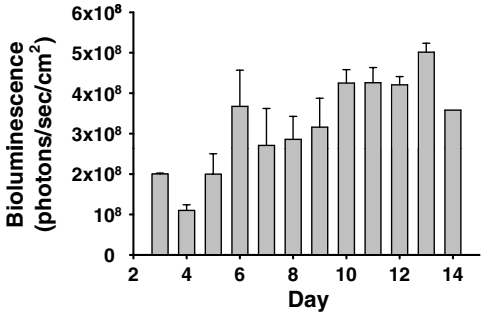

Fig. S6. Stable bioluminescence detection of albumin promoter-driven firefly luciferase expression from reporter HEALs in vitro. Hepatocyte/fibroblast cells cocultivated for 7–10 d were transduced with lentivirus expressing firefly luciferase (Fluc) under the albumin promoter and encapsulated the following day in PEG diacrylate + RGDS hydrogels. Albumin-Fluc reporter HEALs were incubated briefly in 3 mg/mL luciferin/PBS, and bioluminescence imaging was performed using the Xenogen IVIS with Living Systems software to collect peak luminescence flux over 2 wk in vitro. Error bars represent SEM for $n = 3$.

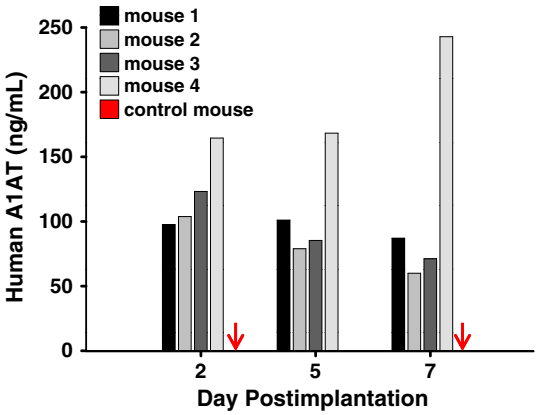

Fig. S7. Detection of human alpha-1-antityrpsin (A1AT) in serum of mice humanized with HEALs over time. Serum samples acquired on day 2, 5, and 7 after implantation in athymic nude mice were assayed for human A1AT by enzyme-linked immunosorbent assay. Plotted are $n = 4$ mice per group, represented by individual bars (mouse 1, 2, 3, 4). Control mouse contains no implant; red arrows indicate that human A1AT was undetectable in these samples.

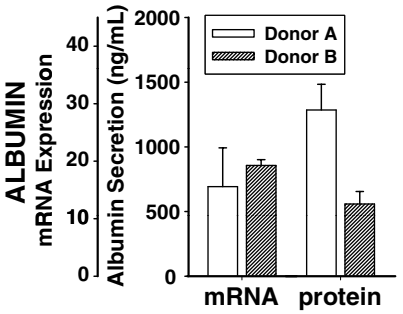

Fig. S8. Characterization of HEALs made from different donors. Cryopreserved primary human hepatocyte lots from donors A or B were cocultivated with fibroblasts (FIB), encapsulated with liver endothelial cells (LEC) in PEG diacrylate + RGDS hydrogels and cultured in hepatocyte medium for 10 d. On day 10 after encapsulation, total RNA was extracted from donor A- or B-derived HEALs, and a LMA Luminex analysis was performed to quantify human albumin mRNA expression ("mRNA") relative to control gene transferrin. Spent media sampled from cultured donor A- or B-derived HEALs was used to quantify human albumin secretion on day 2 after encapsulation ("protein"). Error bars represent SEM for $n = 3$.

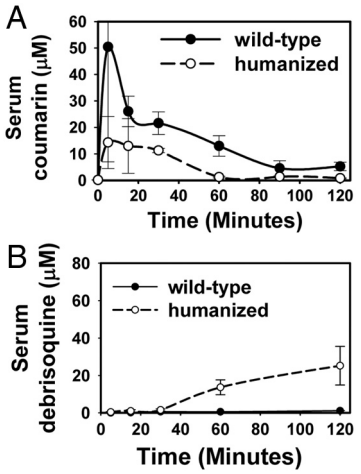

Fig. S9. Pharmacokinetic analysis of parent drugs coumarin and debrisoquine in humanized mice. (*A*) Humanized mice established on a nude mouse background were administered coumarin at 80 mg/kg by intraperitoneal injection, and (*B*) humanized mice established on a C57/Bl6 mouse background were administered debrisoquine at 2 mg/kg by oral gavage. Following drug administration, mice were bled by retroorbital draw at specific time points, and parent and metabolite concentration quantified by liquid chromatography/MS/MS. Open circles represent humanized mice, and closed circles represent wild-type (no implant) mice. Error bars are SEM for $n = 3$ mice per group.

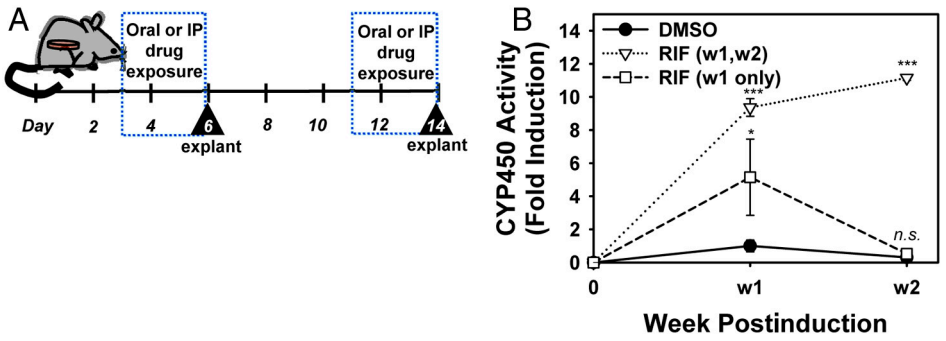

Fig. S10. Utility of humanized mice for predicting human drug responses. (*A*) Timeline of exposure to clinical inducer rifampin (RIF) in vivo, here administered 20 mg/kg by intraperitoneal (IP) injection. (*B*) Dynamics of CYP450 induction in explanted HEALs exposed in vivo to IP-administered RIF over 1 or 2 wk, with a washout period included in week 2 to determine if HEALs were dynamically responsive to both the exposure and clearance of RIF. To assess cytochrome P450 superfamily enzyme (CYP450) activity, humanized mice were administered RIF daily for 3 d before HEAL extraction and incubation with substrate 7-benzyloxy-4-trifluoromethylcoumarin ex vivo. Fold-induction of CYP450 activity was determined by normalization to DMSO control; n.s., not significant; $*p < 0.01$, $**p < 0.05$, $***p < 0.001$ for $n = 6$ mice per group and SEM.

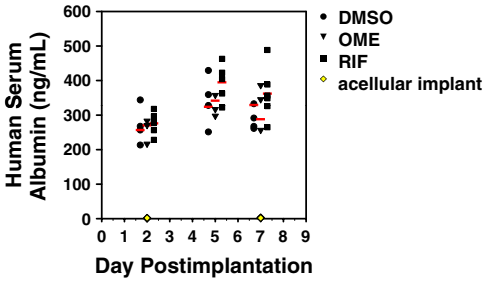

Fig. S11. Human serum albumin from humanized mice is unaffected by exposure to clinical drug inducers over time. Humanized mice were administered DMSO by intraperitoneal injection (●), omeprazole (OME) by oral gavage (40 μM, ▼), or rifampin (RIF) by intraperitoneal injection (25 μM, ■), daily, at days 4–7 after implantation. Blood was collected by retroorbital draw on days 2, 5, and 7 after implantation for drug-treated mice and control mice with acellular hydrogel intraperitoneal implantations. Red bars mark average human serum albumin levels at each time point for $n = 3$–6 mice per condition.

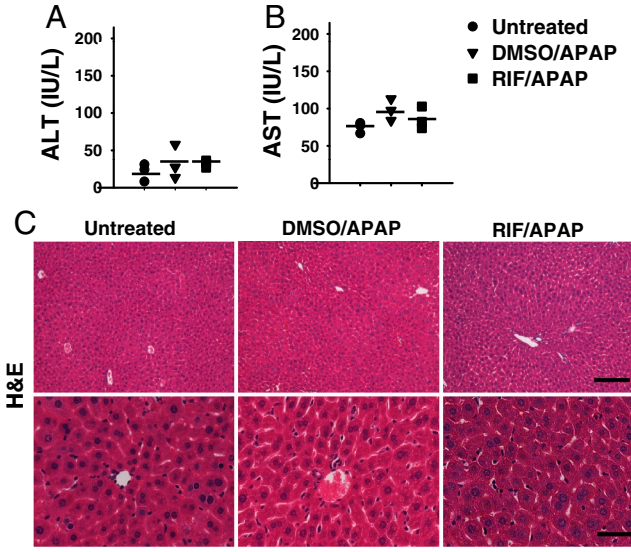

Fig. S12. Serum liver function tests and liver histology for mice exposed to rifampin (RIF) and acetaminophen (APAP) combinations. (*A*–*C*) Humanized mice established for 7 d exposed to no drug ("Untreated," ●) or inducer/drug combinations DMSO/APAP (▼) or RIF/APAP (■). Serum samples acquired at 4 h following APAP exposure were assayed for liver damage markers alanine aminotransferase (ALT) (*A*), and aspartate aminotransferase (AST) (*B*) using an endpoint colorimetric enzymatic assay. Mice per group, $n = 3$; black lines represent average values for each group. Explanted livers were sectioned and stained with hematoxylin and eosin (H&E) (*C*). Representative images are shown. [Scale bars: 270 μm (*Upper*) and 70 μm (*Lower*).]

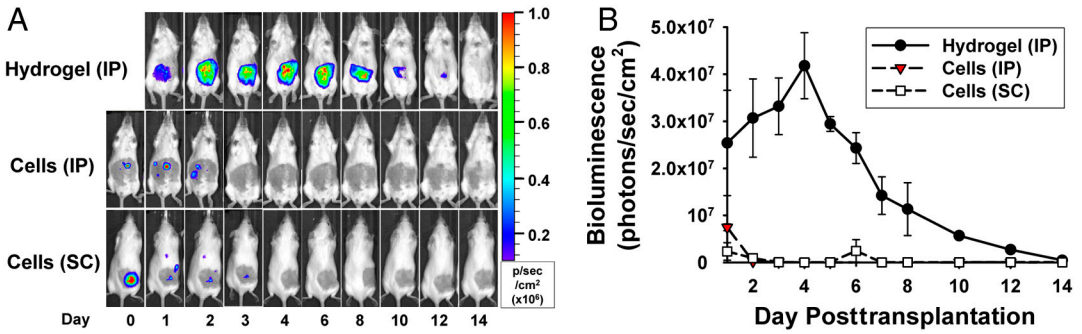

Fig. S13. Implantation of HEALs compared to transplantation of human liver cells in immune-competent Swiss–Webster white mice. (*A* and *B*) Albumin-luciferase-reporter human HEP/FIB cocultures were used for fabrication of reporter albumin-firefly luciferase HEALs implanted in the intraperitoneal cavity of Swiss–Webster mice [Hydrogel (IP)], or for direct transplantation of $\sim 1 \times 10^6$ cocultured hepatocytes in the intraperitoneal cavity [Cells (IP)] or subcutaneous space [Cells (SC)]. Implanted and transplanted mice were injected with 250 μL 15 mg/mL luciferin/PBS solution, and bioluminescence imaging was performed using the Xenogen IVIS with Living Systems software to collect peak in vivo luminescence flux periodically over 2 wk. Representative images (*A*) and quantification of bioluminescence (*B*) are shown for $n = 3$ per group. Error bars represent SEM.

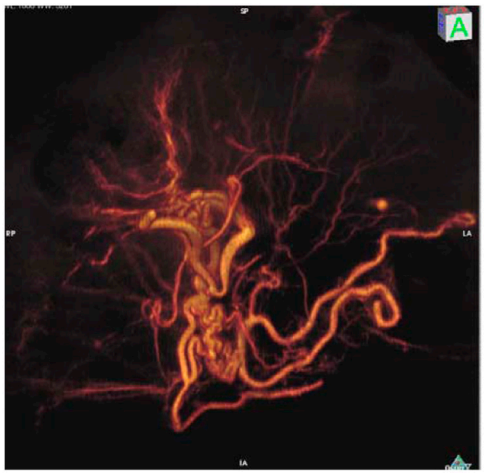

Movie S1. Three-dimensional rendering of mouse vessel permeation in extracted HEAL. Humanized mice were perfused with yellow Microfil silicone rubber agent on day 35 of implantation, and engrafted HEAL was removed and scanned by microcomputed tomography angiography. Rendering was done with Osirix software.

Movie S1 (MOV)

Other Supporting Information Files

Dataset S1 (XLS)